

# Evaluation of Piezocomposites for Ultrasonic Transducer Applications—Influence of the Unit Cell Dimensions and the Properties of Constituents on the Performance of 2-2 Piezocomposites

Xuecang Geng and Q. M. Zhang

**Abstract**—A theoretical model on piezoceramic polymer composites with laminar periodic structure is presented. A salient feature of this model is that it can treat explicitly how the unit cell dimensions and other material properties influence the performance of an ultrasonic transducer made of 2-2 piezocomposites. The model predicts that there exist a series of modes associated with the periodic structure of a composite, which is beyond the stop-band edge resonance prediction. One of the main concerns in designing a composite transducer is how the surface vibration profile changes with frequency and how this is influenced by the aspect ratio of the ceramic plate. It was predicted that as long as the thickness resonance is below the first lateral mode frequency, there is always a frequency  $f_1$  which is near the thickness resonance and at which the polymer and ceramic vibrate in unison. The effect of aspect ratio is to change the position of  $f_1$  with respect to the thickness resonance frequency and the bandwidth in which polymer and ceramic have nearly the same vibration amplitude and phase. It is also predicted that, when operated in a fluid medium such as water, there will be a resonance mode which has a frequency determined by the velocity of the fluid medium and the unit cell length  $d$  and is associated with the oscillation of the fluid. The behavior of a composite plate as an acoustic transmitter and receiver and the influence of the aspect ratio of the ceramic plate on them are also investigated.

## I. INTRODUCTION

TO PRODUCE a high performance ultrasonic transducer requires the transducer material, which performs the energy conversion between the mechanical form and electrical form, to have a high electromechanical coupling factor, broad operation frequency bandwidth, and adjustable acoustic impedance which can be tuned to match that of the medium. With single phase piezoelectric materials, it is difficult to simultaneously meet all the requirements. Piezoceramic polymer composite materials, which combine the high electromechanical activity of piezoceramics and the low acoustic impedance of polymeric materials, have provided new opportunities to meet these requirements [1],

[2]. Since their inception in the seventies, the piezoceramic polymer composites have become one of the most important transducer materials and are being widely used in many areas such as medical imaging, nondestructive evaluation of materials, underwater vision, etc.

Being a diphasic material, the properties of a piezocomposite can be tailored over a wide range by adjusting the material properties and geometric shapes of constituent phases [3], [4]. It has also been observed that the properties of a composite vary with frequency [5]. The challenge of understanding the seemingly complex relationship between the performance of a composite and the properties of its constituents and the great opportunities provided by these materials have stimulated, in the past two decades, extensive investigations, both experimental and theoretical, on this class of materials.

The classic work of Newnham *et al.*, [6] which classified piezocomposite materials according to the connectivity of the constituent phases, has greatly facilitated the analysis of the composites as the connectivity is one of the key parameters in determining the performance of a composite. For composites with 1-3 and 2-2 connectivities, both analytical and finite element modelings have been carried out which have provided useful guidelines in the design of composite transducers [7]–[13]. The isostrain models developed by Smith and Auld [3] and Hashimoto and Yamaguchi [4] linked the material parameters of the constituents to the effective piezoelectric properties of 1-3 and 2-2 composites, respectively, and predicted that the thickness coupling factor  $k_t$  of a composite can approach the longitudinal coupling factor  $k_{33}^l$  of the piezoceramic rod and  $k_{33}^w$  of the plate, respectively, which is in good agreement with experiments for composites with a high aspect ratio  $t/d$ , where  $t$  is the thickness and  $d$  is the periodicity of the composites. Auld *et al.* [7], using the Floquet theory, investigated wave propagations in both the 2-2 and 1-3 composites and showed that, due to the periodic structure of these composites, there exist pass bands and stop bands, similar to the band structure in a crystal solid, and that there are piezoelectric resonances associated with the stop band edge resonances [7]–[10]. For the design of composite transducers, the recognition of the existence of these modes and the precise prediction of their frequencies are of

Manuscript received August 27, 1996; accepted January 14, 1997. This work was supported by the Office of Naval Research under the Grant No: N00014-96-0357.

The authors are with Materials Research Laboratory and Department of Electrical Engineering, Pennsylvania State University, University Park, PA 16802 (e-mail: qxzl@psuvm.psu.edu).

prime importance since, quite often, it is the interference of these modes with the thickness mode of a composite that deteriorates the performance, especially at high frequency operations. Craciun *et al.* [11] examined the coupling between these lateral modes and thickness mode using a phenomenological approach, and the results provided qualitative understanding between the coupling of the two modes and the material properties. The results from these investigations have played important roles in the development of ultrasonic composite transducers. However, due to the approximations used in the analysis, there are severe limitations. For instance, various features related to the dynamic behavior of a composite transducer were not treated in a consistent manner, and the effect of finite thickness of a composite on the material properties, that has been shown to be crucial in determining the performance of a piezocomposite, cannot be treated in these analyses. To address these realistic issues of a composite material, finite element analysis has been employed by many authors [12]–[15]. For example, the dispersion curves have been evaluated for various modes in a composite and the dependence of the electromechanical coupling factor on the ceramic volume content and the ceramic rod shape was investigated.

For a piezoceramic polymer composite, it has to be recognized that it is the ceramic phase which performs the energy conversion between the electric and mechanical forms and the polymer phase merely acts as a carrier which transfers acoustic energy between the piezoceramic and the external medium. Hence, if the elastic coupling between the two constituents is not very effective, even if the material exhibits a perfect acoustic impedance matching with the medium and the electromechanical coupling factor is large, the electromechanical performance of the material is still poor. These observations clearly indicate that in modeling piezoceramic polymer composites, one cannot simply use an effective medium approach and has to take into account explicitly this internal degree of freedom.

Recently, we developed an analytical model on the dynamic problem of a piezocomposite material with the 2-2 connectivity [16]–[18]. In the model, we avoided the approximations made in the earlier works and, hence, can address the dynamic responses of 2-2 piezocomposites, such as the frequencies of various modes, the mode coupling, the electromechanical coupling factor, the vibration profiles of composites under different external driving conditions, etc., in a realistic and consistent manner. For example, one of the misconceptions in the early studies of the dynamic behavior of piezocomposites is the direct linkage between the non-uniform surface vibration profile in a composite and the aspect ratio of the ceramic plate (in 2-2 composites) or rod (in 1-3 composites). Here, we will show, which was verified by experiment, that for a composite plate, as long as the thickness resonance frequency is below that of the lateral mode, there is always a frequency near the thickness resonance where the vibration profile of the composite is uniform. The influence of the

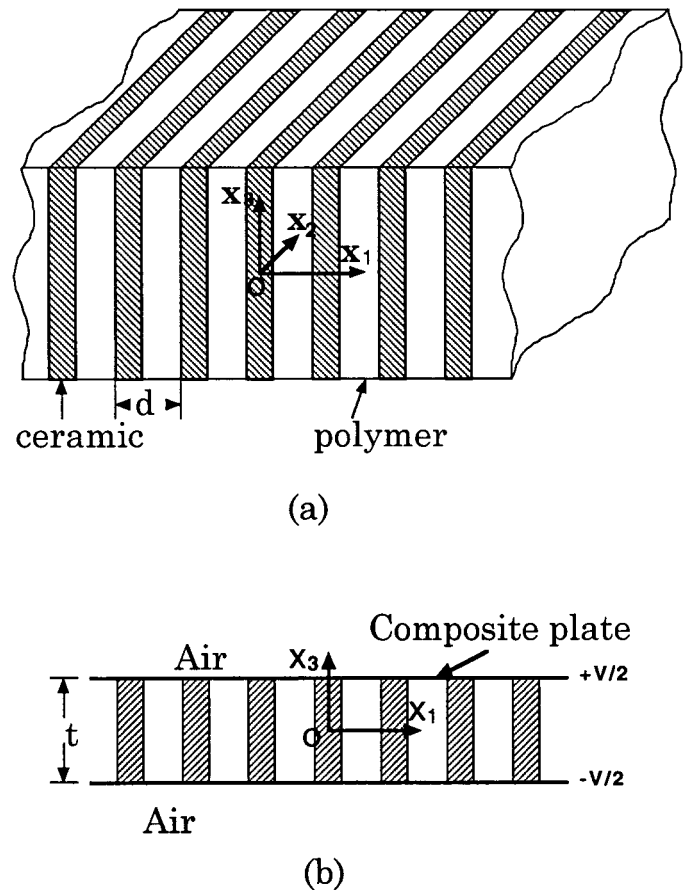


Fig. 1. (a) Schematic drawing of a 2-2 piezoceramic polymer composite which is unbounded in all three orthogonal directions. The period of the composite is  $d$ . (b) Schematic drawing of a 2-2 piezoceramic polymer composite plate with a thickness  $t$  situated in air. An external voltage is applied to the composite.

aspect ratio is on the frequency bandwidth in which the polymer and ceramic vibrate in unison.

The approach taken here to solve the vibration problem in a finite thickness composite plate is based on the method of partial wave expansion where the various elastic and electric fields are expanded in terms of the eigenmodes of the structure as shown in Fig. 1(a) and the coefficients for each eigen-mode are determined by the boundary conditions at  $x_3 = t/2$  [Fig. 1(b)]. Some of the results have been presented in early publications. In this paper, we would like to summarize briefly these early results and then, discuss many issues pertinent to the design of piezocomposite ultrasonic transducers based on the results from the model analysis. The paper is organized as the following: First, the details of derivation of the eigenfunctions for a 2-2 piezoceramic polymer composite will be presented. Based on the results, the wave propagation in an unbounded 2-2 composite is analyzed. For the finite thickness composites, various features of a piezocomposite plate under an external driving electric field in both air and water media are treated. The response behavior of the composite plate under external pressure is also treated. Experiments were conducted to provide comparison with the theoretical re-

sults. From the results, we will show explicitly how the aspect ratio  $t/d$  influences the transduction performance of a composite plate.

## II. GENERAL SOLUTIONS FOR WAVE PROPAGATION IN A 2-2 PIEZOCOMPOSITE

Shown in Fig. 1(a) is a schematic drawing of a 2-2 composite (unbounded in the  $x_3$ -direction), where plates of piezoceramic and polymer form a parallel array. The coordinate system is chosen such that the  $x_3$ -axis is along the ceramic poling direction, the  $x_1$ -axis is perpendicular to the ceramic polymer interface, and  $x_2$ -axis is in the plane of the plates. For a typical 2-2 composite, the dimensions in the  $x_1$ - and  $x_2$ -directions are much larger than the period  $d$  and thickness  $t$ . In the treatment here, they can be taken as infinite without much error in the results. Under these conditions, the composite is clamped in the  $x_2$ -direction so that  $S_2 = 0$ , where  $S_2$  is the strain in the  $x_2$ -direction, and the problem becomes a two-dimensional one with no dependence on the  $x_2$ -coordinate.

The governing equations for the dynamics of a 2-2 composite are [19]–[21]:

$$\begin{aligned} \frac{\partial T_1}{\partial x_1} + \frac{\partial T_5}{\partial x_3} &= \rho \frac{\partial^2 u_1}{\partial t^2} \\ \frac{\partial T_5}{\partial x_1} + \frac{\partial T_3}{\partial x_3} &= \rho \frac{\partial^2 u_3}{\partial t^2} \\ \frac{\partial D_1}{\partial x_1} + \frac{\partial D_3}{\partial x_3} &= 0. \end{aligned} \quad (1)$$

The symbols adopted in this paper are summarized here:  $T_i$  and  $S_i$  are the stress and strain tensor components, where the Voigt notation is used,  $u_i$  is the elastic displacement vector,  $\rho$  is the density, and  $D_i$  is the electric displacement vector,  $E_i$  is the electric field. The relevant material coefficients are:  $e_{ij}$  is the piezoelectric coefficient,  $c_{ij}$  is the elastic stiffness, and  $\varepsilon_i$  is the dielectric permittivity. Equation (1) holds for both the polymer and ceramic phases.

The constitutive equations, relating stress  $T$ , strain  $S$ , electric displacement  $D$ , and electric field  $E$ , are:

$$[T] = [c^E][S] - [e_t][E] \quad (2a)$$

$$[D] = [e][S] + [\varepsilon^S][E]. \quad (2b)$$

For the polymer phase,  $e_{ki}$  in (2) are zero. The superscripts  $E$  and  $S$  indicate that the coefficients are under the constant  $E$  field and constant strain conditions, respectively. Here  $[e_t]$  is the transposed  $[e]$  array. Under the quasi-electrostatic approximation, the electric field  $E$  can be expressed as:

$$\vec{E} = -\nabla\Phi \quad (3)$$

where  $\Phi$  is the electrical potential.

Combining (1), (2), and (3) yields three second order differential equations, governing the elastic displacement

$u_1$ ,  $u_3$ , and electric potential  $\Phi$  in the ceramic plate, respectively:

$$\begin{aligned} c_{44}^E u_{3,11} + (c_{13}^E + c_{44}^E) u_{1,13} + c_{33}^E u_{3,33} \\ + (e_{33}\Phi_{,33} + e_{15}\Phi_{,11}) &= \rho \ddot{u}_3 \\ c_{11}^E u_{1,11} + (c_{13}^E + c_{44}^E) u_{3,13} + c_{44}^E u_{1,33} \\ + (e_{31} + e_{15})\Phi_{,13} &= \rho \ddot{u}_1 \\ e_{15} u_{3,11} + (e_{15} + e_{31}) u_{1,13} + e_{33} u_{3,33} \\ - (\varepsilon_{33}^S \Phi_{,33} + \varepsilon_{11}^S \Phi_{,11}) &= 0. \end{aligned} \quad (4)$$

For the polymer phase,  $e_{ij}$  in (4) should be taken to zero.

For an unbounded composite, the solutions to (4) have the form:

$$\begin{aligned} u_3 &= A \exp(j(hx_1 + \beta x_3 - \omega t)) \\ u_1 &= B \exp(j(hx_1 + \beta x_3 - \omega t)) \\ \Phi &= C \exp(j(hx_1 + \beta x_3 - \omega t)) \end{aligned} \quad (5)$$

where  $A$ ,  $B$ , and  $C$  are three constants,  $\omega$  is the angular frequency,  $h$  and  $\beta$  are the wave vector components in the  $x_1$ - and  $x_3$ -directions, respectively.

Substituting (5) into (4) yields three homogeneous equations with the undetermined constants  $A$ ,  $B$ , and  $C$ ,

$$[M_{ij}][A_i] = 0 \quad (6)$$

where  $[A_i] = [A, B, C]^T$  and

$$[M_{ij}] = \begin{pmatrix} c_{33}^E \beta^2 + c_{44}^E h^2 - \rho \omega^2 & (c_{13}^E + c_{44}^E) h \beta & e_{33} \beta^2 + e_{15} h^2 \\ (c_{13}^E + c_{44}^E) h \beta & c_{11}^E h^2 + c_{44}^E \beta^2 - \rho \omega^2 & (e_{15} + e_{31}) h \beta \\ e_{33} \beta^2 + e_{15} h^2 & (e_{15} + e_{31}) h \beta & -(\varepsilon_{11}^S h^2 + \varepsilon_{33}^S \beta^2) \end{pmatrix}. \quad (7)$$

The condition for a nontrivial solution is such that the determinant of the coefficient matrix vanishes, i.e.,

$$|M_{ij}| = 0 \quad (8)$$

Equation (8) is a cubic equation of  $h^2$ . For a given  $\omega$  and  $\beta$ , (8), in general, has three roots of  $h^2$ , denoted as  $h_1^c$ ,  $h_2^c$ , and  $h_3^c$ , corresponding to the quasi-electromagnetic, quasi-longitudinal, and quasi-shear waves in the piezoelectric plate, respectively. For each  $h_i^c$ , the ratio among  $A$ ,  $B$ , and  $C$  can be determined from (6). Since we are concerned only with the waves in the  $x_3$  direction which correspond to piezo-active modes in a finite thickness composite plate, the general solutions become:

$$\begin{aligned} u_3^c &= \sum_i R_i^c f_i^c \cos(h_i^c x_1) \sin(\beta x_3) \\ u_1^c &= \sum_i R_i^c g_i^c \sin(h_i^c x_1) \cos(\beta x_3) \\ \Phi^c &= \sum_i R_i^c t_i^c \cos(h_i^c x_1) \sin(\beta x_3) \end{aligned} \quad (9)$$

where  $i$  runs from 1 to 3.  $f_i$ ,  $g_i$  and  $t_i$  are the cofactors of  $A_{k1}(i)$ ,  $A_{k2}(i)$ , and  $A_{k3}(i)$  of the determinant (8) (where

$h$  is replaced by  $h_i^c$  for  $i = 1, 2$ , and  $3$ , respectively). The  $\exp(-j\omega t)$  term in (9) is omitted.

Following the similar procedure, the solutions for the polymer phase can be obtained (the center of the polymer plate is at  $x_1 = d/2$ ):

$$\begin{aligned} u_3^P &= \sum_i R_i^P f_i^P \cos\left(h_i^P\left(x_1 - \frac{d}{2}\right)\right) \sin(\beta x_3) \\ u_1^P &= \sum_i R_i^P g_i^P \sin\left(h_i^P\left(x_1 - \frac{d}{2}\right)\right) \cos(\beta x_3) \\ \Phi^P &= C^P \cosh\left(\beta\left(x_1 - \frac{d}{2}\right)\right) \sin(\beta x_3) \end{aligned} \quad (10)$$

where  $i = 1, 2$ .  $f_i^P$  and  $g_i^P$  are the cofactors of  $A_{k1}(i)$ ,  $A_{k2}(i)$  of the determinant (8) with all the material parameters replaced by those of the polymer phase, and

$$(h_1^P)^2 = (k_L^P)^2 - \beta^2 \text{ and } (h_2^P)^2 = (k_T^P)^2 - \beta^2$$

where  $k_L^P = \frac{\omega}{\nu_L^P}$ ,  $k_T^P = \frac{\omega}{\nu_T^P}$ ,  $\nu_L^P$ , and  $\nu_T^P$  are the longitudinal and shear wave velocities of the polymer phase, respectively.

The expressions of the stresses and the electric displacement in the ceramic plate can be obtained by substituting (9) into (2):

$$\begin{aligned} T_1^C &= \sum_i T_{11}^C(i) R_i^C \cos(h_i^C x_1) \cos(\beta x_3) \\ T_3^C &= \sum_i T_{33}^C(i) R_i^C \cos(h_i^C x_1) \cos(\beta x_3) \\ T_5^C &= \sum_i T_{31}^C(i) R_i^C \sin(h_i^C x_1) \sin(\beta x_3) \end{aligned} \quad (11)$$

where

$$\begin{aligned} T_{11}^C(i) &= c_{11}^E h_i^C g_i^C + (c_{13}^E f_i^C + e_{31} t_i^C) \beta \\ T_{33}^C(i) &= c_{33}^E h_i^C g_i^C + (c_{33}^E f_i^C + e_{33} t_i^C) \beta \\ T_{31}^C(i) &= -c_{44}^E (\beta g_i^C + h_i^C f_i^C) - e_{15} h_i^C t_i^C \end{aligned} \quad (12)$$

where  $i = 1, 2, 3$  for ceramic phase. The electric displacements are:

$$D_1^C = \sum_i D_1^C(i) R_i^C \sin(h_i^C x_1) \sin(\beta x_3) \quad (13a)$$

$$D_3^C = \sum_i D_3^C(i) R_i^C \cos(h_i^C x_1) \cos(\beta x_3) \quad (13b)$$

where  $D_1^C(i) = -e_{15}(\beta g_i^C + h_i^C f_i^C) + \varepsilon_{11}^E h_i^C t_i^C$  and  $D_3^C(i) = e_{31} h_i^C g_i^C + e_{33} \beta f_i^C - \varepsilon_{33}^E \beta t_i^C$ . Similar expressions can be obtained for the polymer plate. For instance, the electric displacements are:

$$D_1^P = -\varepsilon_{11}^P \beta C^P \sinh\left(\beta\left(x_1 - \frac{d}{2}\right)\right) \sin(\beta x_3) \quad (14a)$$

$$D_3^P = -\varepsilon_{11}^P \beta C^P \cosh\left(\beta\left(x_1 - \frac{d}{2}\right)\right) \cos(\beta x_3) \quad (14b)$$

Making use of the boundary conditions at the ceramic polymer interface ( $x_1 = \nu d/2$ , where  $\nu$  is the volume fraction of the ceramic in a composite), which are:

$$u_1^C = u_1^P, u_3^C = u_3^P, T_1^C = T_1^P \text{ and } T_5^C = T_5^P \quad (15a)$$

$$\text{and } \Phi^C = \Phi^P \text{ and } D_1^C = D_1^P \quad (15b)$$

$R_i^C$ ,  $R_j^P$  and  $C^P$ . ( $i = 1, 2, 3$  and  $j = 1, 2$ ) can be determined. Expanding (15) in terms of (9), (10), (11), (13), and (14) yields the following six homogeneous linear equations:

$$\begin{pmatrix} K_{11} & K_{12} & K_{13} & K_{14} & K_{15} & 0 \\ K_{21} & K_{22} & K_{23} & K_{24} & K_{25} & 0 \\ K_{31} & K_{32} & K_{33} & K_{34} & K_{35} & 0 \\ K_{41} & K_{42} & K_{43} & K_{44} & K_{45} & 0 \\ 0 & 0 & K_{53} & K_{54} & K_{55} & K_{56} \\ 0 & 0 & K_{63} & K_{64} & K_{65} & K_{66} \end{pmatrix} \begin{pmatrix} R_1^P \\ R_2^P \\ R_1^C \\ R_2^C \\ R_3^C \\ C^P \end{pmatrix} = 0 \quad (16)$$

where the matrix elements  $K_{ij}$  are functions of  $\beta$ ,  $\omega$ ,  $d$ ,  $\nu$ , and the material parameters of both the polymer and piezoceramic. The condition that the determinant

$$|K_{ij}| = 0 \quad (17)$$

yields the relationship between  $\omega$  and  $\beta$ , the dispersion relations in the composite. For each pair of  $\omega$  and  $\beta$ , the relationships among  $R_i^C$ ,  $R_j^P$ , and  $C^P$  can be obtained. Hence, the various stress, strain, electric field distributions in the composite can be determined.

### III. DISPERSION CURVES, MODES, AND MODES COUPLING OF A 2-2 PIEZOCOMPOSITE

Equation (17) allows us to determine the relationship between  $\beta$  and  $\omega$ , the dispersion curves, for a composite if the materials parameters of piezoceramic and polymer and the geometric parameters, such as  $d$  and  $\nu$ , are known. Equation (17) is a transcendental function which cannot be solved analytically. A computer code was developed and the dispersion curves were evaluated numerically.

Shown in Fig. 2 (the solid curves) are the two lowest branches of the dispersion curves for a 2-2 composite made of PZT-5H piezoceramic and Spurr epoxy with the ceramic volume fraction of 44%.<sup>1</sup> For all the composites discussed in this paper, except otherwise specified, PZT-5H piezoceramic and Spurr epoxy are used as the constituents. The parameters of PZT-5H and Spurr epoxy are presented in Table I. The general trend of the dispersion curves in Fig. 2 resembles that of the symmetric Lamb waves in a plate [19]. As will be shown later, at small  $\beta d$  limit, the first branch corresponds to the longitudinal wave propagation along the  $x_3$ -direction, that is,  $u_3$  is the dominant displacement which is more or less uniform and in phase in the  $x_1$ -direction, and its phase velocity is the effective longitudinal

<sup>1</sup>PZT-5H is the trade-mark of Morgan Mattroc Inc., Bedford, OH 44146, for one of its PZT piezoceramics. Spurr epoxy is the trade-mark of Polysciences, Inc., Warrington, PA 18976.

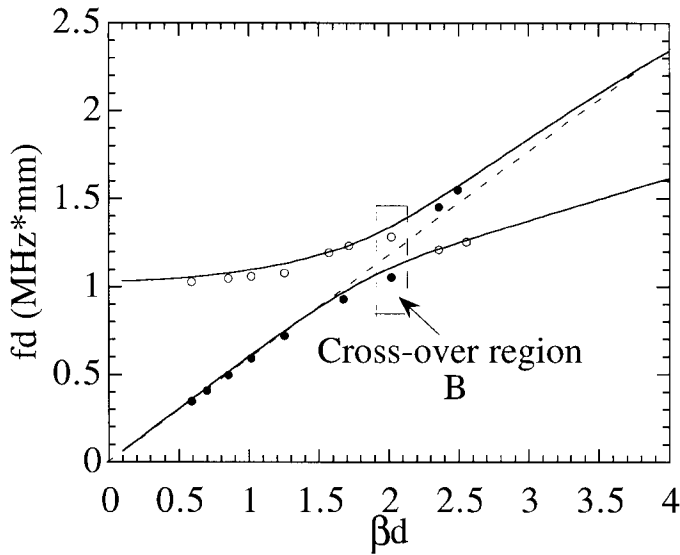


Fig. 2. The first and second branches of the dispersion curves (solid lines) and the experimentally measured thickness mode (solid circles) and lateral mode (open circles) for a 2-2 composite made of PZT-5H and Spurr epoxy with 44% ceramic content. After the crossover region, the thickness mode jumps to the second branch. The criterion for the thickness mode is that it is the one with the larger effective coupling factor.

TABLE I

THE MATERIAL PROPERTIES OF PZT-5H AND SPURR EPOXY USED FOR THE 2-2 COMPOSITES IN THE INVESTIGATION.

PZT-5H: $e_{33} = 23.09 \text{ C/m}^2$ , $e_{31} = -6.603 \text{ C/m}^2$ , $e_{15} = 17.0 \text{ C/m}^2$ , $c_{11} = 12.72 * 10^{10} \text{ N/m}^2$ , $c_{44} = 2.3 * 10^{10} \text{ N/m}^2$ , $c_{33} = 11.74 * 10^{10} \text{ N/m}^2$ , $c_{13} = 8.47 * 10^{10} \text{ N/m}^2$ , $K_{11} = 1700$ , $K_{33} = 1470$ , $\rho = 7500 \text{ kg/m}^3$ . Spurr epoxy: $c_{11} = 5.4 * 10^9 \text{ N/m}^2$ , $c_{44} = 1.3 * 10^9 \text{ N/m}^2$ , $\rho = 1100 \text{ kg/m}^3$ .
---

wave velocity of the composite. The second branch corresponds to the lateral resonance which arises from the periodic structure of the composite, that is, it is a stationary shear wave along the  $x_1$ -direction, and it can be shown that the displacement  $u_3$  of the polymer phase is much larger than that of the ceramic phase and the phase difference between them is  $180^\circ$ . Hence, it is the so-called stop-band edge resonance as predicted by Auld *et al.* [7], [8].

Under the assumption that the wave length  $\lambda$  in the  $x_3$ -direction ( $\beta = 2\pi/\lambda$ ) is equal to two times the composite thickness  $t$  (the condition for the thickness resonance), the theoretical dispersion curves can be compared with the experimental results, obtained from composites with different thickness. At low  $\beta d$  on the dispersion curves, where  $d$  is the period of the composite, the frequency of the fundamental thickness mode from the experiment falls on the first branch as marked by the black dots, and the frequency of the first lateral mode falls on the second branch as marked by the open circles. After the crossover region B, the modes interchange the positions on the dispersion curves where the thickness mode is in the second branch while there is a weak resonance at a frequency below the

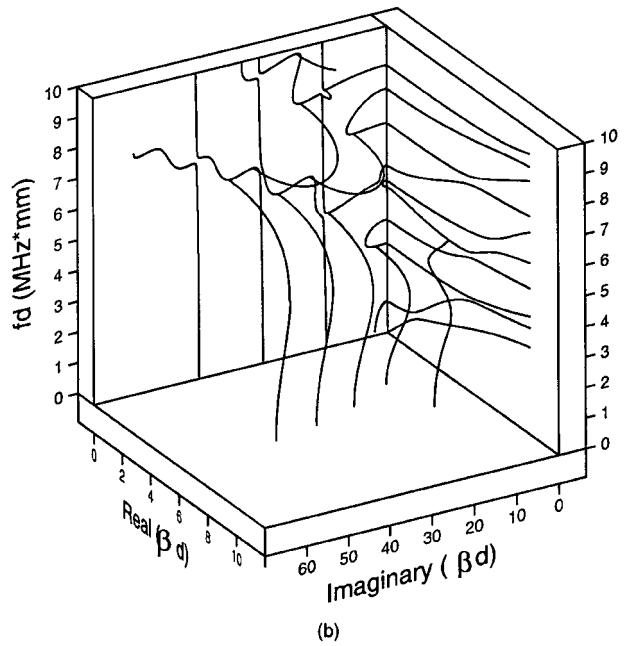
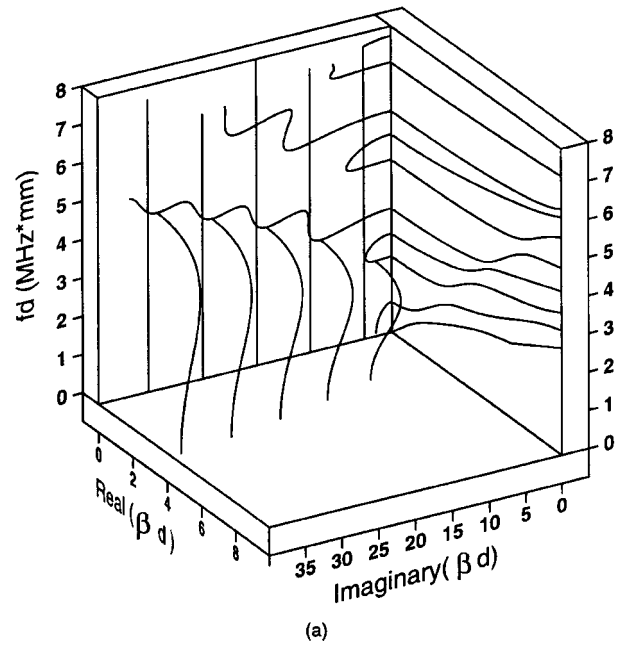


Fig. 3. The dispersion curves for a 2-2 composite [Fig. 1(a)] made of PZT-5H and Spurr epoxy for (a) 15% ceramic volume content and (b) 44% ceramic volume content.

thickness mode, and it falls on the first branch. Here, the thickness mode is defined as the one with higher electromechanical coupling factor. The mode on the first branch gradually diminishes at high  $\beta d$  values. The result is presented in Fig. 2. Clearly, there is an excellent accord between the theoretically derived resonance frequencies and experimentally observed ones.

Shown in Figs. 3(a) and 3(b) are the 3-dimensional dispersion curves for 2-2 composites with 15% and 44% ceramic volume fraction, respectively. Obviously, there are imaginary and complex branches of the dispersion curves. The modes on these branches are non-propagating

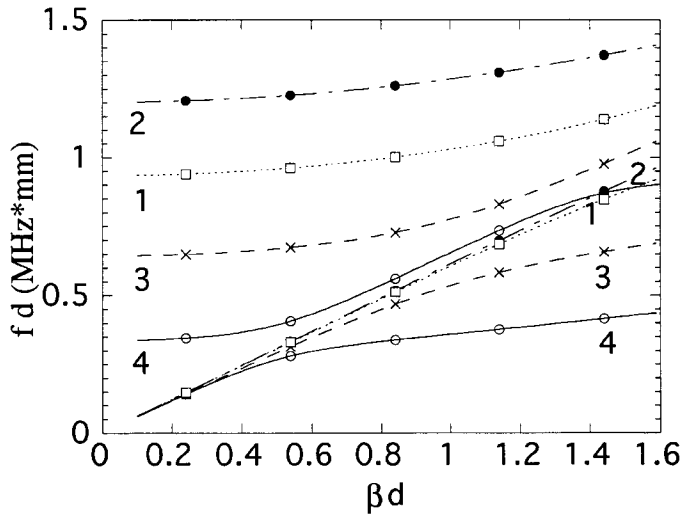


Fig. 4. The effect of the properties of the polymer matrix on the dispersion curves of 2-2 composites with PZT-5H ceramic, derived from the model. The properties of the polymer phase are: curve 1:  $c_{11} = 7.72 \times 10^9$  N/m<sup>2</sup>,  $c_{44} = 1.588 \times 10^9$  N/m<sup>2</sup>,  $\rho = 1160$  kg/m<sup>3</sup>; curve 2:  $c_{11} = 1.3634 \times 10^{10}$  N/m<sup>2</sup>,  $c_{44} = 3.432 \times 10^9$  N/m<sup>2</sup>,  $\rho = 1610$  kg/m<sup>3</sup>; curve 3:  $c_{11} = 3.173 \times 10^9$  N/m<sup>2</sup>,  $c_{44} = 0.696 \times 10^9$  N/m<sup>2</sup>,  $\rho = 1060$  kg/m<sup>3</sup>; curve 4:  $c_{11} = 1.622 \times 10^9$  N/m<sup>2</sup>,  $c_{44} = 1.646 \times 10^8$  N/m<sup>2</sup>,  $\rho = 890$  kg/m<sup>3</sup>.

modes (imaginary branches) and attenuated modes (complex branches), respectively. These modes do not exist in an unbounded composite, however, they are important in the vibration problems of finite thickness plates as well as in semi-infinite mediums, where they correspond to the evanescent waves at the surface which will be discussed later in the paper.

Fig. 4 presents the effect of the stiffness of the polymer phase on the dispersion curves of a 2-2 composite with 30% ceramic content where PZT-5H is used as the piezoceramic phase. It is apparent that the frequency position of the second branch is very sensitive to properties of the polymer phase. This is quite understandable since, as will be shown later, the frequency position of this branch is directly related to the shear velocity of the polymer matrix for composites at this ceramic content. The lower the shear wave velocity of the polymer phase is, the lower the frequency of the second branch will be. Therefore, for a transducer operated at high frequencies, in order to avoid the interference from the lateral modes, a polymer matrix with a high shear velocity should be utilized even though the thickness coupling factor  $k_t$  of this composite may be reduced as a result of the stiffer polymer matrix [3], [4].

In order to further elucidate the origins of these resonant modes, it is instructive to make a comparison between the dispersion curves of a composite and those of single piezoceramic and polymer plates with appropriate boundary conditions [22]. In general, in piezoceramic polymer composites, the elastic stiffness of the piezoceramic is more than one order of magnitude higher than that of the polymer. It is reasonable to assume that the piezoceramic plates in a 2-2 composite are stress free at the ceramic-polymer interface, that is, the stress components  $T_1$  and  $T_5$

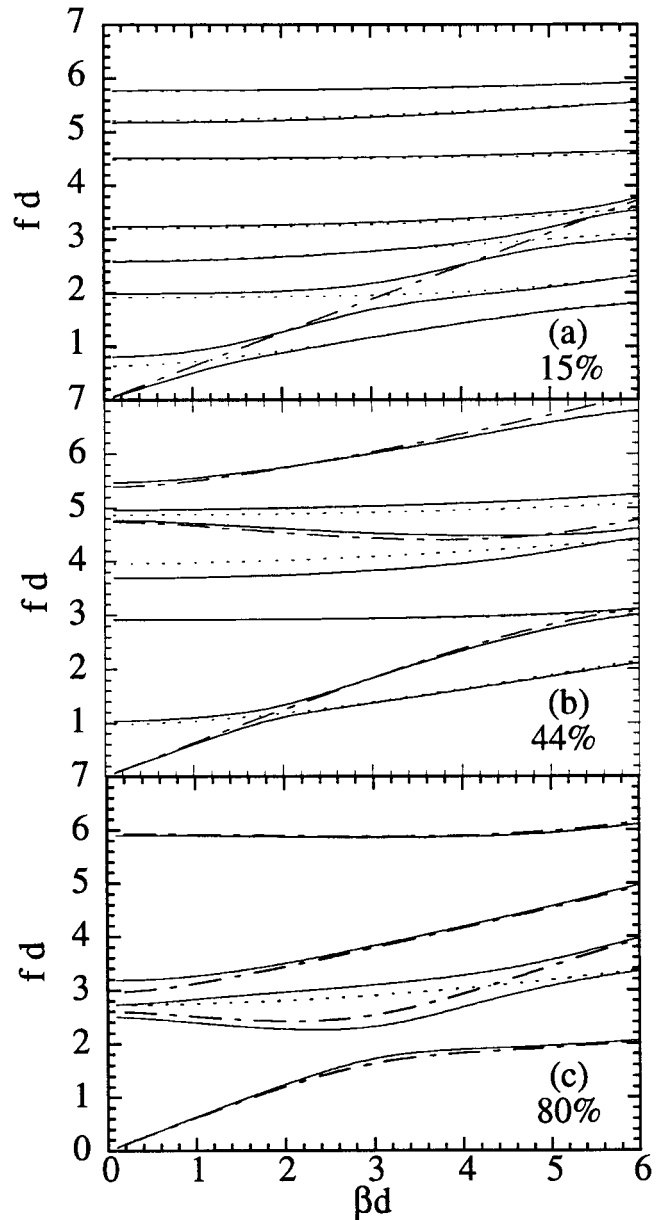


Fig. 5. Comparison of the dispersion curves in 2-2 composites with those in a single piezoceramic plate and a polymer plate for composites with (a) 15% ceramic content; (b) 44% ceramic; and (c) 80% ceramic content. PZT-5H is used as the piezoceramic and Spurr epoxy as the polymer phase.

are zero at the interface. Similarly, the polymer plates can be approximated as under the fixed boundary conditions, that is,  $u_1$  and  $u_3$  are zero at the interface. Under these assumptions, the dispersion curves of both single ceramic and single polymer plates are calculated for the plates with different widths corresponding to 2-2 composites with different ceramic volume fractions. The results are presented in Figs. 5(a), 5(b), and 5(c) corresponding to 2-2 composites with 15%, 44%, and 80% ceramic content, respectively. In these figures, the solid lines are the dispersion curves of the 2-2 composites, the dashed lines are those of the ceramic plate, and dotted lines are the dispersion curves of the polymer plate.

The results from these figures reveal that there are many resemblances between the dispersion curves of 2-2 composites and the dispersion curves of the single ceramic and single polymer plates with appropriate boundary conditions. For instance, at small  $\beta d$ , the first branch in the dispersion curves of the 2-2 composites with 44% and 80% ceramic volume content is very close to the first branch of the ceramic plate. On the other hand, for 2-2 composites with low ceramic volume content, a large difference between these two is found for the first branch. These results are consistent with those from Smith and Auld [3] and from Hashimoto and Yamaguchi [4] based on an effective medium model. For the second branch which corresponds to the lateral resonant mode in a composite plate, at low and medium ceramic volume content, it is close to the first branch of the polymer plate which frequency at small  $\beta d$  is equal to  $V_T^P/2d_P$  where  $V_T^P$  and  $d_P$  are shear wave velocity and width of the polymer plate, respectively. However, for composites with high ceramic volume content such as the one shown here (80%), the second branch is related to the longitudinal resonance of the ceramic plate along the width- (or  $x_1$ -) direction while the shear resonance associated with the polymer plate lies on the third branch of the dispersion curves.

Obviously, the coupling between the two phases through the interface boundary conditions will influence the dispersion curves of the waves in the two phases. It is well known that the dispersion curves for the uncoupled waves are split at their crossover points when coupling is introduced [11]. Far from the crossover region, the coupled wave dispersion curves should nearly coincide with those of the uncoupled waves. If the coupling is very strong as for the 15% and 44% piezocomposites, the coupled waves exhibit large departure from the uncoupled curves in the crossover region, which is clearly shown in Figs. 5(a) and 5(b). While for the composite with 80% ceramic content, the coupling between the first and the second branches is through the coupling of P wave and SV wave in the ceramic plate where the interface does not have a significant effect on it.

#### IV. VIBRATION OF A FINITE THICKNESS COMPOSITE PLATE UNDER AN ELECTRIC FIELD IN AIR

In the previous section, the properties of guided wave propagation in laminated 2-2 piezocomposites have been analyzed. In spite of the fact that many effective parameters of the material can be derived by this simple method, one key issue in the design of a composite transducer, i.e., the influence of the aspect ratio of the ceramic plates (or the unit cell) in a composite on the performance of the transducer cannot be addressed. In this section, we will treat the vibration problem of a finite thickness composite plate under an external driving electric field and situated in air. From the analysis, one can obtain detailed information on how the surface vibration profile changes with frequency and its dependence on the aspect ratio of the ceramic plate (or the unit cell dimension), the possible resonant modes in a composite transducer, and the de-

pendence of the electromechanical coupling factor on the aspect ratio of the ceramic plate, etc. We will also show that, as long as the thickness resonance frequency is below the lateral mode frequency, the aspect ratio will not have a direct effect on the vibration uniformity of a composite near the thickness resonance. The influence is on the bandwidth in which the ceramic and polymer vibrate with nearly the same amplitude and phase.

A composite plate with a thickness  $t$  is drawn schematically in Fig. 1(b). For the problem treated here, the two free surfaces of the composite plate are electroded with conducting material and an AC electric field of a frequency  $f$  is applied between the two electrodes.

It is well known that there exist no simple solutions for the vibration problem of a finite thickness plate such as the piezocomposite treated here. One of the most frequently used approximation methods is to expand the elastic and electric fields in a material in terms of the eigenfunctions in an unbounded one [21]. Different techniques such as the variational technique and the method of least squares can be used to determine the expansion coefficients. For the composite plate treated here, we found that the variational technique is more appropriate in treating the boundary problem than the method of least squares because of the large difference in the vibration amplitudes between the two phases in the composite.

For the ceramic phase in the composite plate, the elastic displacements  $u_3$  and  $u_1$ , and the electric potential  $\Phi$  are expanded in terms of the eigenfunctions derived:

$$\begin{aligned} u_3^C &= \sum_{n=1}^m \sum_{i=1}^3 R_{ni}^C f_{ni}^C \cos(h_{ni}^C x_1) \sin(\beta_n x_3) A_n \\ u_1^C &= \sum_{n=1}^m \sum_{i=1}^3 R_{ni}^C g_{ni}^C \sin(h_{ni}^C x_1) \cos(\beta_n x_3) A_n \\ &\quad + C R_0^C \sin(h_{01}^C x_1) \\ \Phi^C &= \sum_{n=1}^m \sum_{i=1}^3 R_{ni}^C t_{ni}^C \cos(h_{ni}^C x_1) \sin(\beta_n x_3) A_n + C x_3. \end{aligned} \quad (18)$$

Similarly, for the polymer phase in the composite plate:

$$\begin{aligned} u_3^P &= \sum_{n=1}^m \sum_{i=1}^2 R_{ni}^P f_{ni}^P \cos\left(h_{ni}^P \left(x_1 - \frac{d}{2}\right)\right) \sin(\beta_n x_3) A_n \\ u_1^P &= \sum_{n=1}^m \sum_{i=1}^2 R_{ni}^P g_{ni}^P \sin\left(h_{ni}^P \left(x_1 - \frac{d}{2}\right)\right) \cos(\beta_n x_3) A_n \\ &\quad + C R_0^P \sin\left(h_{01}^P \left(x_1 - \frac{d}{2}\right)\right) \\ \Phi^P &= \sum_{n=1}^m C_n^P \cosh\left(\beta_n \left(x_1 - \frac{d}{2}\right)\right) \sin(\beta_n x_3) A_n + C x_3 \end{aligned} \quad (19)$$

where  $R_{n1}^C$ ,  $R_{n2}^C$ ,  $R_{n3}^C$ ,  $R_{n1}^P$ ,  $R_{n2}^P$ , and  $C_n^P$  are determined in (16),  $\beta_n$ ,  $h_{ni}^C$ , and  $h_{ni}^P$  are the wave vector components of the  $n$ th mode in the  $x_3$ - and  $x_1$ -directions where the superscripts  $c$  and  $p$  stand for the ceramic and polymer, respectively.  $h_{01}^C$  and  $h_{01}^P$  are related to the mode in which

$\beta$  is equal to zero:  $h_{01}^C = \sqrt{\frac{E^C}{c_{11}^C}}\omega$  and  $h_{01}^P = \sqrt{\frac{E^P}{c_{11}^P}}\omega$ .  $R_0^C$  and  $R_0^P$  are determined by (16) in which  $\beta$  is set to zero. The mode with  $\beta = 0$  is generated due to the fact that the velocity of the electromagnetic wave is much faster than that of the elastic waves and the composite plate is clamped in the  $x_3$ -direction ( $S_3 = 0$ ).  $A_n$  and  $C$  are the coefficients which will be determined by the boundary conditions which are traction free and  $\Phi = \pm V/2$  (here  $\exp(-j\omega t)$  is omitted) at  $x_3 = \pm t/2$ .

The stresses  $T_3$ ,  $T_5$  and electric displacement  $D_3$  are expressed as:

$$T_3^C = \sum_{n=1}^m \sum_{i=1}^3 T_{33}^C(n, i) \cos(h_{ni}^C x_1) \cos(\beta_n x_3) A_n + (e_{33} + T_0^C \cos(h_{01}^C x_1)) C \quad (20a)$$

$$T_5^C = \sum_{n=1}^m \sum_{i=1}^3 T_{13}^C(n, i) \sin(h_{ni}^C x_1) \sin(\beta_n x_3) A_n \quad (20b)$$

$$D_3^C = \sum_{n=1}^m \sum_{i=1}^3 D_3^C(n, i) \cos(h_{ni}^C x_1) \cos(\beta_n x_3) A_n + (-\varepsilon_{33}^S + D_0^C \cos(h_{01}^C x_1)) C \quad (20c)$$

$$T_3^P = \sum_{n=1}^m \sum_{i=1}^2 T_{33}^P(n, i) \cos\left(h_{ni}^P \left(x_1 - \frac{d}{2}\right)\right) \cos(\beta_n x_3) A_n + T_0^P \cos\left(h_{01}^P \left(x_1 - \frac{d}{2}\right)\right) C \quad (20d)$$

$$T_5^P = \sum_{n=1}^m \sum_{i=1}^2 T_{13}^P(n, i) \sin\left(h_{ni}^P \left(x_1 - \frac{d}{2}\right)\right) \sin(\beta_n x_3) A_n \quad (20e)$$

$$D_3^P = \sum_{n=1}^m \sum_{i=1}^2 D_3^P(n, i) \cos\left(h_{ni}^P \left(x_1 - \frac{d}{2}\right)\right) \cos(\beta_n x_3) A_n - \varepsilon_{11}^P C \quad (20f)$$

where  $T_{33}^C(n, i)$ ,  $T_{13}^C(n, i)$ ,  $D_3^C(n, i)$ ,  $T_{33}^P(n, i)$ ,  $T_{13}^P(n, i)$ , and  $D_3^P(n, i)$  are the same as  $T_{33}^C(i)$ ,  $T_{31}^C(i)$ ,  $D_3^C(i)$ ,  $T_{33}^P(i)$ ,  $T_{31}^P(i)$ , and  $D_3^P(i)$  in (11) to (14) if the subscript  $i$  there is replaced by  $n$  and  $i$  for  $i$ -th partial wave of  $n$ -th mode here. And

$$T_0^C = c_{13}^E h_{01}^C R_0^C, \quad T_0^P = c_{12}^P h_{01}^P R_0^P, \quad D_0^C = e_{31} h_{01}^C R_0^C.$$

The number of the eigenfunctions,  $m$ , required in the expansion is determined by the accuracy needed for the solution. For the problem treated here, we found that it is adequate to use eight eigen-modes in the expansion. In the frequency range studied ( $fd < 2$  MHz\*mm), there are two branches having real  $\beta$  and the other branches having either imaginary or complex  $\beta$ , which corresponds to the modes confined at the surface of  $x_3 = \pm t/2$ .

For the problem treated here, all the stress components in air are zero and for the sake of simplicity,  $D$  in air is also assumed to be zero since the dielectric permittivity of the composite is much higher than air. Under these conditions,

the variational formula takes the following form:

$$\int_V [(T_{kl,k} - \rho \ddot{u}_l) \delta u_l^* + D_{k,k} \delta \Phi^*] dV + \int_S [(-T_{kl}) \delta u_l^* + (\Phi - \bar{\Phi}) \delta D_k^*] dS = 0 \quad (21)$$

where the integration over time has been performed to take into account the complex notations for the quantities in the integrands [19], [21]. The  $*$  represents the complex conjugate of the corresponding quantity. The first integral is over the volume of the 2-2 composite plate, and it can be shown that it is equal to zero since all the quantities in the integrand satisfy (1). The second integral is over the surfaces of the composite plate at  $x_3 = \pm t/2$  where  $\bar{\Phi} = \pm V/2$  at  $x_3 = \pm t/2$  where  $V$  is the applied voltage. The periodic condition of the composite in the  $x_1$ -direction and the symmetric condition of the solutions and the boundary conditions about the plane of  $x_3 = 0$  allow the second integration to be performed over one unit cell at  $x_3 = t/2$ .

Substituting  $T_3$ ,  $T_5$ ,  $u_1$ ,  $u_3$ ,  $\Phi$ , and  $D_3$  into (21) yields the following linear algebraic equation:

$$(M_{ij})(A_j) = (V_i) \quad (22)$$

where  $(M_{ij})$  is a  $9 \times 9$  matrix,  $(A_j) = (A_1, A_2, A_3, A_4, A_5, A_6, A_7, A_8, C)^T$ ,  $(V_i)$  is a  $9 \times 1$  matrix whose elements depend only on  $V$ , the applied voltage. For a given frequency  $f$ , one can solve (22) to obtain  $A_j$  and  $C$ . From  $A_j$  and  $C$ , (18), (19), and (20) yield all the characteristic properties related to the vibration of a 2-2 composite plate with different thickness and different ceramic volume fraction such as the electrical impedance, surface displacement distribution, resonant modes, electromechanical coupling coefficient, etc.

For the composite plate treated here, the electrical impedance for a single repeating unit can be found from:

$$Z = \frac{V}{I} \quad (23)$$

where  $I$  is the current which is equal to  $I = \frac{dQ}{dt} = -j\omega Q = -j2\omega b \int_0^{d/2} D_3 dx_1$ , where  $Q$  and  $b$  are the electric charge and the length in the  $x_2$ -direction of the plate, respectively. To compare with the experimental result, the current  $I$  should be multiplied by  $N$ , the number of repeating unit in a composite plate.

Shown in Fig. 6(a) is the electric impedance curve calculated from (22) and (23) for a composite plate with  $t/d = 4.5$  and the ceramic volume fraction  $\nu = 44\%$ . The electric impedance measured experimentally from the same composite plate is shown in Fig. 6(b) and clearly the theoretical impedance curve reproduces the experimental data quite well. The difference in the sharpness of the resonant peaks between the experimental data and the theoretical curve is due to the fact that in the theoretical analysis, the electrical and mechanical losses of the ceramic and polymer phases were not included.

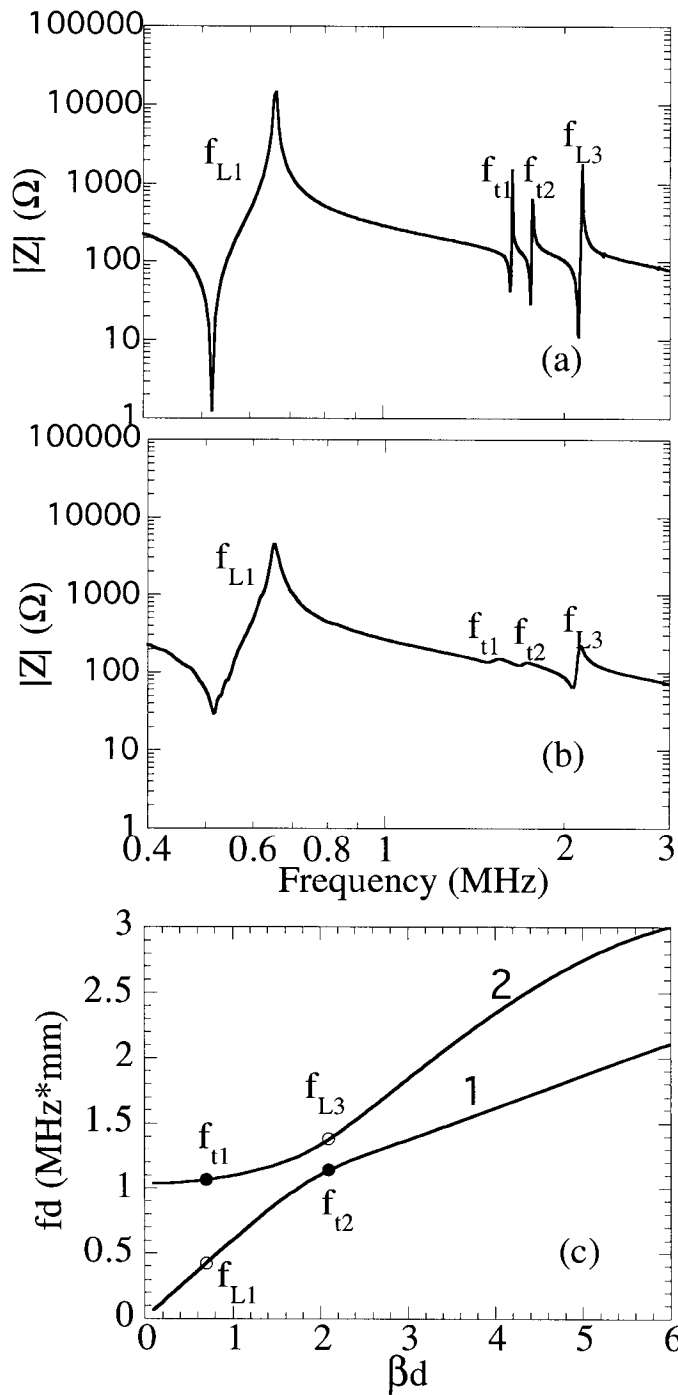


Fig. 6. The electric impedance curve for a 2-2 composite plate with PZT-5H and Spurr epoxy (44% ceramic) measured in air: (a) the theoretical curve and (b) the experimental curve. The thickness  $t$  of the composite is  $t/d = 4.5$  and  $d = 0.635$  mm.  $f_{L1}$  and  $f_{L3}$  are the fundamental and third harmonic of the thickness mode and  $f_{t1}$  and  $f_{t2}$  are the modes arose from the periodicity of the composite. (c) The dispersion curves elucidating the origin of the resonant modes  $f_{t1}$  and  $f_{t2}$ . In general, any modes on the dispersion curves will show up whenever  $\beta d = (2n + 1)/2$ ,  $n = 0, 1, 2, \dots$  is satisfied, where  $\beta = 2\pi/\lambda$  and  $\lambda = 2t$ .

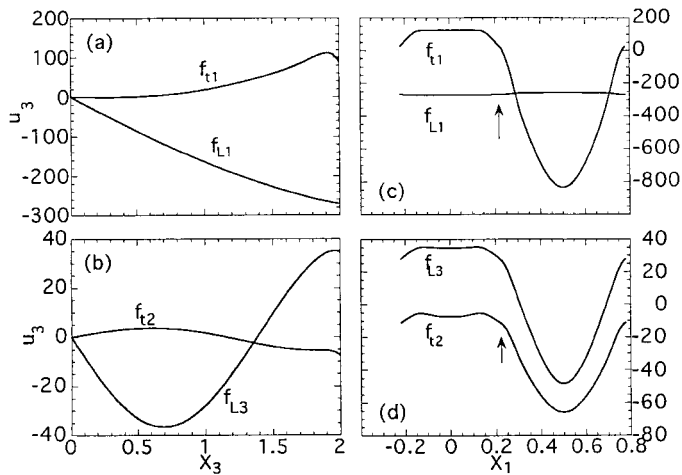


Fig. 7. The distribution of the elastic displacement  $u_3$  for  $f_{L1}$ ,  $f_{L3}$ ,  $f_{t1}$ , and  $f_{t2}$  of a 2-2 composite with  $t/d = 4$ , where (a) and (b) are the distributions along the  $x_3$ -direction when  $x_1 = 0$  [at the center line of the ceramic plate, Fig. 1(b)],  $x_3 = 0$  is at the center and  $x_3 = 2$  is at the ceramic surface; (c) and (d) are surface vibration profiles at  $x_3 = 2$ ,  $x_1 = 0$  corresponds to the center of the ceramic plate and  $x_1 = 0.5$  is at the center of the polymer plate.

In Fig. 6(c), the peak positions from the experimental data are compared with the dispersion curves for this composite which shows excellent agreement between the two. In order to elucidate the nature of these modes, the spatial distribution of  $u_3$  at each mode at the composite surface is presented in Fig. 7 which are evaluated based on (18) and (19). Apparently,  $f_{L1}$  is the fundamental thickness resonance and  $f_{t1}$  is the first lateral mode as revealed by the fact that the ceramic and polymer vibrate  $180^\circ$  out of phase at this mode, as predicted in the earlier theoretical work [7], [8]. The frequency position and the distribution of  $u_3$  along the  $x_3$  axis indicate that  $f_{L3}$  is the third harmonic of the thickness mode. However, the appearance of  $f_{t2}$  is not expected from the earlier theoretical works in which the ceramic and polymer vibrate in phase. By examining the equations of the boundary conditions at  $x_3 = \pm t/2$ , it can be deduced that a resonance will occur whenever  $\beta = (1 + 2n)\pi/t$ , i.e.,  $\cos(\beta t/2) = 0$ . Hence, the dispersion curves of real  $\beta$ , as shown in Fig. 6(c), reveal that the fundamental thickness resonance and the first lateral resonance occur at  $\beta = \pi/t$  ( $f_{L1}$  and  $f_{t1}$ ). Similarly, when  $\beta = 3\pi/t$ , the third harmonic of the thickness mode will occur at  $f_{L3}$ . In addition, a mode  $f_{t2}$  will also show up at the branch 1 which is at a frequency near and above  $f_{t1}$ . By the same argument, it would be expected that  $f_{L5}$ ,  $f_{t3}$ , etc. may also be observed, depending on the electromechanical coupling factors of these modes. As shown later, the effective coupling factor for the modes in the first branch will decrease with increasing  $\beta d$ , i.e., reducing thickness, and on the other hand, the effective coupling factor for the modes in the second branch will increase with  $\beta$ . As the ratio of  $t/d$  decreases, the frequency of the thickness mode will gradually move toward the first lateral mode which will become stronger (coupling factor increases), and the second lateral mode ( $f_{t2}$ ) becomes weaker and finally it

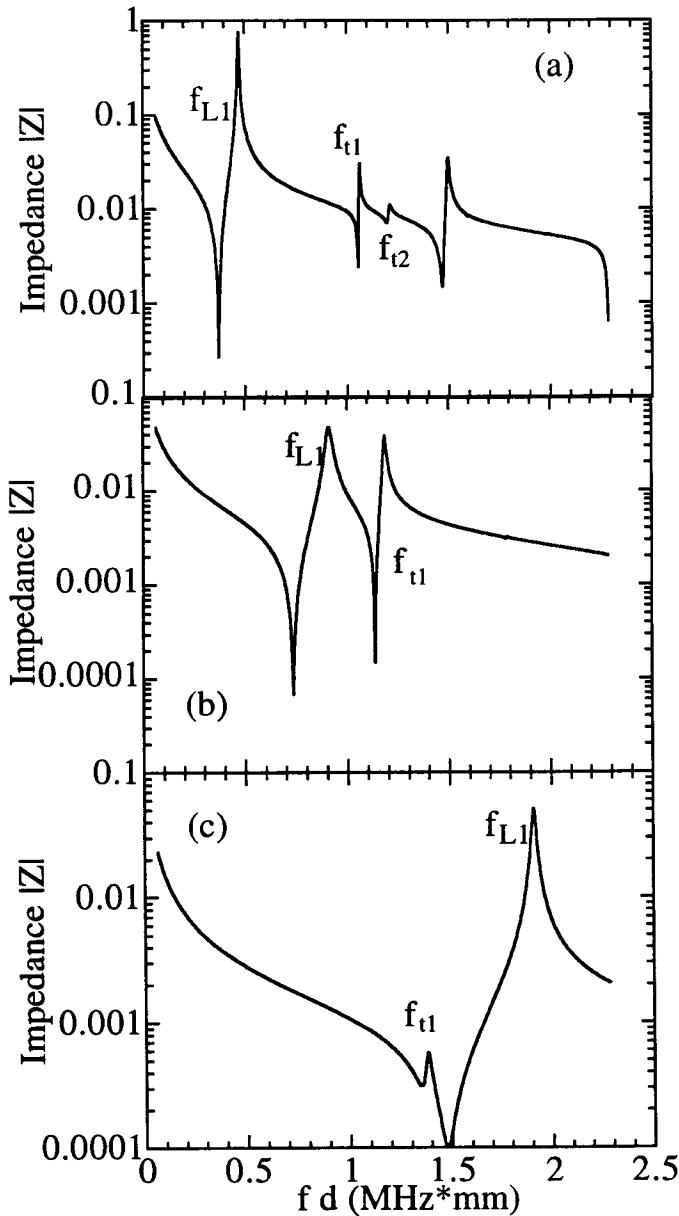


Fig. 8. The evolution of various modes in a 2-2 composite made of PZT-5H (44% ceramic) and Spurr epoxy with the thickness  $t$  of composite plate: (a)  $t/d = 4$ , (b)  $t/d = 2$ , and (c)  $t/d = 1$ . There is already substantial coupling between the thickness and lateral modes at  $t/d = 2$  for this composite. At low  $t/d$  values (thin samples), the lateral mode will disappear.

will disappear. These features are summarized in Fig. 8 which provide understanding on the earlier experimental observations on how various modes change with temperature (which causes reduction of the shear velocity of the polymer phase) and the composite thickness [5].

Both the experimental results and the theoretical data indicate that the ceramic and polymer vibrate in phase for all the modes on the first branch and out of phase for modes on the second branch.

The electromechanical coupling factor for the thickness resonance can be evaluated based on the definition

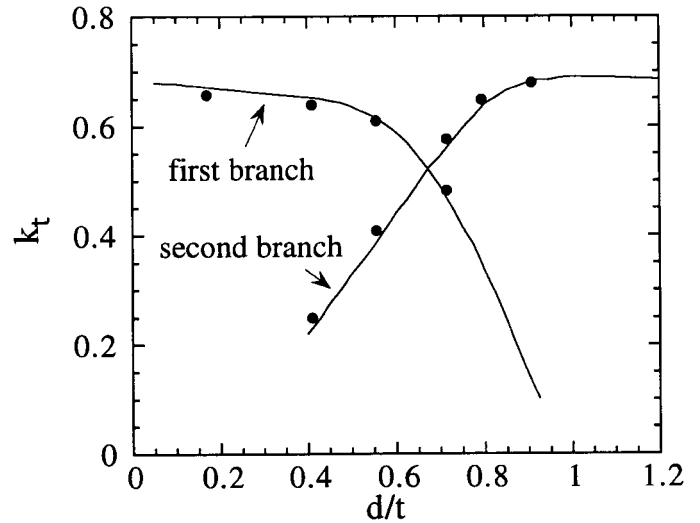


Fig. 9. The evolution of the coupling factor for the modes on the first and second branches of the dispersion curves with the composite thickness  $d/t$  for a composite made of PZT-5H and Spurr epoxy with 44% ceramic content.

of IEEE [20]:

$$k_t^2 = \frac{\pi f_s}{2 f_p} \tan\left(\frac{\pi f_p - f_s}{2 f_p}\right) \quad (24)$$

where  $k_t$  is the thickness mode coupling factor,  $f_s$  and  $f_p$  are the series and parallel resonance frequencies, respectively. Equation (24) is used here to calculate the coupling factor for the modes in both the first and second branches. Shown in Fig. 9 are the results for a 2-2 composite plate with 44% ceramic volume content for different  $d/t$ , where both theoretical and experimental results are presented. As the ratio of  $d/t$  increases, the coupling factor of the mode (thickness mode) in the first branch gradually decreases, while the coupling factor of the mode in the second branch gradually increases due to the modes coupling. As  $d/t$  increases further, the thickness mode will jump to the second branch when the coupling factor in the second branch surpasses that of the first branch. Although in this region the coupling factor for the thickness mode can still be quite high, the distribution of  $u_3$  is not uniform on the composite surface and the ceramic and polymer vibrate  $180^\circ$  out of phase, which is not desirable since the polymer phase will not be able to perform properly the function of transferring the acoustic energy between the ceramic plates and the external medium.

For a composite plate to work effectively as an electromechanical transduction material, it is required that the ceramic and the polymer plates in the composite vibrate in phase with nearly the same amplitude in the  $x_3$ -direction. The evolution of the vibration pattern in the two phases with frequency and the effect of the aspect ratio  $t/d$  of a composite plate on this distribution are investigated. Shown in Fig. 10(a) is the variation of the ratio  $u_3^P/u_3^C$  at the surface of the composite plate, where  $u_3^P$  and  $u_3^C$  are  $u_3$  at the centers of the polymer ( $x_1 = d/2$ ) and the ceramic plates ( $x_1 = 0$ ), respectively, with frequency

for the composite plate of  $t/d = 4$  where both the experimental results and theoretically calculated curve are presented. The experimental data were acquired using a laser dilatometer [23]. Hence, at frequencies far below any resonant mode,  $u_3^P/u_3^C$  is always less than one, which is true as long as the composite is driven electrically. For a given frequency, as  $t/d$  increases, this ratio increases and approaches one. These are consistent with the results of the earlier theoretical work on the static properties of composites [24]. As frequency increases, the ratio  $u_3^P/u_3^C$  increases toward one. At a frequency  $f_1$  which is near  $f_s$  of the thickness mode,  $u_3^P/u_3^C = 1$ . This ratio will surpass one as the frequency is further increased. This is true as long as  $f_{L1} < f_{t1}$ . In Fig. 10(b), the change of  $f_1/f_s$  vs. the ratio of  $d/t$  is presented. Clearly,  $f_1/f_s$  is close to, but larger than, one except for composite plates with a small aspect ratio. Hence, the aspect ratio  $t/d$  does not have a significant effect on the ratio of  $u_3^P/u_3^C$  at frequencies very near  $f_s$  of the thickness mode, where  $u_3^P/u_3^C$  is always near one if the thickness mode is below the first lateral mode frequency. However, it will affect the bandwidth in which  $u_3^P/u_3^C$  is near one. For example, the bandwidth  $\Delta f/f_1$ , where  $\Delta f$  is defined here as the frequency width in which  $0.9 < u_3^P/u_3^C < 1.1$ , increases as the ratio of  $d/t$  decreases, which is shown in Fig. 10(b). The experimental data points are also presented in Fig. 10(b) and the agreement between the two is quite good.

## V. FORCED VIBRATION OF A PIEZOCOMPOSITE PLATE IN A FLUID MEDIUM

Following a similar procedure as outlined in the preceding section, the vibration problem of a composite plate in a fluid medium can also be analyzed, which are more relevant to the practical design and application of a composite transducer. The fluid medium chosen for the study is water and two situations will be investigated: the composite plate as a transmitter, i.e., under a harmonic electric field, and the composite as a receiver, i.e., under a harmonic acoustic pressure in water.

### A. Forced Vibration of a Composite Plate in Water under an AC Electric Field

For the sake of convenience, we will treat the system as a symmetric one in which the composite plate is loaded by water on both surfaces, hence, the boundary conditions at the composite-water interface are:

$$T_3^{Cm} = T_3^W, T_5^{Cm} = 0, u_3^{Cm} = u_3^W \quad \text{and} \quad \Phi = \pm \frac{V}{2} \quad \text{at} \quad x_3 = \pm \frac{t}{2} \quad (25)$$

where superscripts  $Cm$  and  $W$  denote the quantities in the composite and water, and the factor  $e^{-j\omega t}$  is omitted in electric potential  $\Phi$ . The variational formula for this

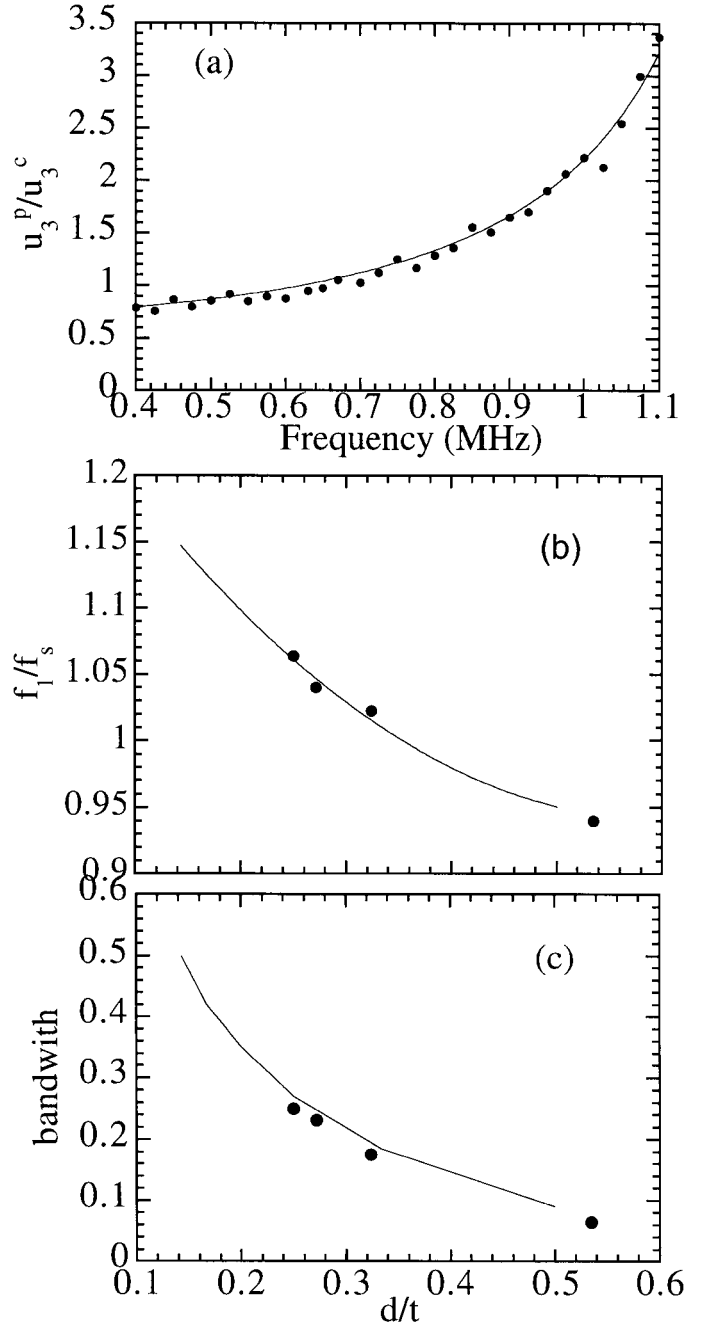


Fig. 10. (a) The ratio of  $u_3^P/u_3^C$  vs. frequency for a composite made of PZT-5H and Spurr epoxy (44% ceramic content) at a thickness of  $t/d = 4$  ( $d = 0.635$  mm) measured in air.  $u_3^P$  and  $u_3^C$  are the surface displacements at the centers of the polymer plate and ceramic plate, respectively. The black dots are the experimental data measured using a laser dilatometer and the solid line is derived from the model. (b) The ratio  $f_1/f_s$  as a function of the ratio  $d/t$  of the composite plate, where  $f_1$  is the frequency at which  $u_3^P/u_3^C = 1$  and  $f_s$  is the series resonant frequency for the thickness mode. The black dots are experimental data and the solid lines are derived from the model calculation. (c) The bandwidth as a function of the ratio  $d/t$  of the composite plate. The black dots are experimental data and the solid lines are derived from the model calculation.

problem can be derived as:

$$\int_{S^\pm} \frac{1}{2} [(T_3^W - T_3^{Cm})(\delta(u_3^W)^* + \delta(u_3^{Cm})^*) + (u_3^{Cm} - u_3^W)(\delta(T_3^W)^* + \delta(T_3^{Cm})^*)] dS + \int_{S^\pm} [(\Phi^{Cm} - \bar{\Phi})\delta(D_3^{Cm})^* - T_5^{Cm}\delta(u_1^{Cm})^*] dS = 0 \quad (26)$$

where  $S^\pm$  indicates that the integration is over the two composite-water interfaces (at  $x_3 = \pm t/2$ ), and the integration over the volume has been omitted since it is equal to zero.

Here, the expressions for the elastic displacement vectors and the electrical potential  $\Phi$  in the composite are those in (18) and (19). Because of the periodic nature of the composite plate in the  $x_1$ -direction, the solutions in water have the form:

$$\begin{aligned} u_1^W &= j \sum_{n=0}^J h_n^W \sin(h_n^W x_1) \exp(\pm j \beta_n^W x_3) R_n^W \\ u_3^W &= \sum_{n=0}^J \beta_n^W \cos(h_n^W x_1) \exp(\pm j \beta_n^W x_3) R_n^W \\ T_3^W &= j T_0^W \sum_{n=0}^J \cos(h_n^W x_1) \exp(\pm j \beta_n^W x_3) R_n^W \end{aligned} \quad (27)$$

where  $h_n^W = \frac{2n\pi}{d}$ ,  $\beta_n^W = \sqrt{\frac{\omega^2}{(V^W)^2} - (h_n^W)^2}$ ,  $T_0^W = c^W(\beta_0^W)^2$ ,  $\beta_0^W = \frac{\omega}{V^W}$ ,  $V^W = \sqrt{\frac{c^W}{\rho^W}}$  is the longitudinal wave velocity of water,  $c^W$  is the bulk modulus of water.  $\pm$  correspond to the solutions in  $x_3 > 0$  region and  $x_3 < 0$  region, respectively.  $h$  and  $\beta$  are the wave vector components in the  $x_1$ - and  $x_3$ -directions in water.  $R_n^W$  is determined by the boundary conditions through the variational principle formula (26).

Substituting (18), (19), and (27) into (26) yields a set of linear algebraic equations:

$$(M_{ij})(A_j) = (V_i) \quad (28)$$

where  $(M_{ij})$  is a matrix in which its elements are related to the parameters of water, ceramic, and polymer and the geometrical parameters  $\nu$  and  $d$ , as well as  $\omega$ ,  $\beta$ , and  $h$ .  $(A_j) = (A_1, \dots, A_m, C, R_0^W, \dots, R_J^W)$ , where  $m$  and  $J$  are the numbers of the eigenfunctions used in the expansions for the quantities in the composite and in water, respectively, and how many eigenfunctions should be used in the expansion depends on the accuracy desired. In this calculation,  $m = 8$  and  $J = 6$ . Hence,  $(V_i)$  is a  $16 \times 1$  matrix which elements depend on the applied voltage  $V$ . Equation (28) is solved numerically.

Shown in Fig. 11(a) is a theoretical electrical impedance curve for a 2-2 composite plate of 44% ceramic volume content and the aspect ratio  $t/d = 3.8$  loaded with water. For the comparison, the experimental curve for the

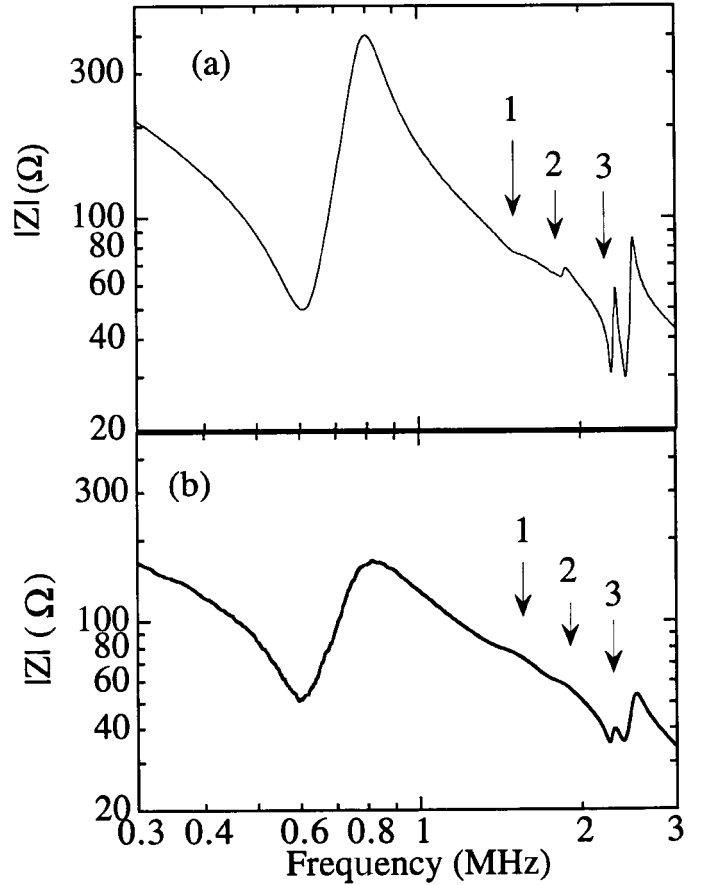


Fig. 11. The electrical impedance magnitude for a 2-2 composite of PZT-5H and Spurr epoxy with 44% ceramic content measured in water. The thickness of the composite is  $t/d = 3.8$  and  $d = 0.635$  mm. (a) is derived from the model and (b) is the experimental results. The modes 1 and 2 are the lateral modes [ $f_{t1}$  and  $f_{t2}$  in Fig. 6(c)] and mode 3 arises from the coupling of water to the periodic structure of the composite surface.

same composite plate is shown in Fig. 11(b). The agreement between the experimental result and the theoretical one is quite good. The relatively sharp resonant peaks in the theoretical curve compared with the experimental one are due to the fact that in the theoretical calculation, the elastic and dielectric losses of the composite plate are not included. Comparison between Fig. 11 with Fig. 6, which is the electrical impedance for a similar composite plate in air, reveals that the resonance is severely damped in water as shown by the marked broadening of the resonant peaks in the impedance curve. For the lateral modes (modes 1 and 2 in Fig. 11) which is mainly determined by the shear resonance of the polymer phase in the 2-2 composite investigated, because the acoustic impedance between the polymer and water is very close, the change in the amplitude is quite significant. One interesting feature of the influence of the water loading on a composite plate is the appearance of a mode which is labeled 3 in Fig. 11. It can be shown that the resonant frequency for this mode does not change very much as the thickness of the composite plate changes. From the stress distribution pattern in the water, it is not difficult to show that this mode is related to

the coupling between the composite and water, and its frequency is determined by the periodicity  $d$  and the acoustic wave velocity of water ( $f = V^w/d$ ). And it corresponds to the local oscillation of water within one unit cell.

In analogous to the situation in air, it is also found that in water, at frequencies far below any resonant mode, the ratio of  $u_3^P/u_3^C$  is always less than one and will approach one as the aspect ratio  $t/d$  increases. As the frequency increases toward the thickness resonant frequency,  $u_3^P/u_3^C$  increases toward one. At a frequency  $f_1$  near the thickness resonant frequency  $f_s$ , this ratio becomes one and above that, this ratio is larger than one [Fig. 12(a)]. Fig. 12(b) presents  $f_1/f_s$  and  $\Delta f/f_1$  vs. the ratio of  $d/t$  for a composite with 44% ceramic content. Clearly, the effect of the aspect ratio  $t/d$  on the surface uniformity of a composite plate is to change the frequency position  $f_1$  with respect to the thickness resonance and the frequency width  $\Delta f$  in which  $u_3^P/u_3^C$  is near one which are very similar to that found in air. However, the bandwidth  $\Delta f/f_1$  in water is larger than that in air, indicating that the surface distribution of the displacement of the two phases is much flatter in water than in air which is quite understandable. Because of the water loading, the vibration amplitude of the polymer phase is significantly reduced. Fig. 12(a) shows how the ratio of  $u_3^P/u_3^C$  at the composite surface varies with frequency ( $t/d = 4$ ). One noticeable change between the surface profiles in air and in water is that in water, even at the lateral mode frequency, this ratio does not become very large (not shown in Fig. 12 since the lateral mode frequency is at about 1.5 MHz).

### B. Forced Vibration of a Composite Plate in Water under Harmonic Acoustic Pressure

Now we turn to investigate the vibration behavior of a composite plate in water under harmonic acoustic pressure, that is, to study issues related to the receiving sensitivity of a simple 2-2 composite transducer. For simplicity, we shall restrict the treatment to the symmetric system. In this case, as sketched in Fig. 13, the incident acoustic waves impinge normally on the two surfaces of the composite plate from opposite directions and the boundary conditions for this problem are:

$$T_3^{Cm} = T_3^W, T_5^{Cm} = 0, u_3^{Cm} = u_3^W \quad \text{and} \quad D_3^{Cm} = 0 \text{ at } x_3 = \pm \frac{t}{2}. \quad (29)$$

The appropriate variational formula is:

$$\int_{S^\pm} \frac{1}{2} [(T_3^W - T_3^{Cm})(\delta(u_3^W))^* + \delta(u_3^{Cm})^*] + (u_3^{Cm} - u_3^W)(\delta(T_3^W))^* + \delta(T_3^{Cm})^*] dS - \int_{S^\pm} [D_3^{Cm} \delta(\Phi^{Cm})^* + T_5^{Cm} \delta(u_1^{Cm})^*] dS = 0. \quad (30)$$

The expressions of the displacements and electrical potential in the composite plate are those in (18) and (19) except

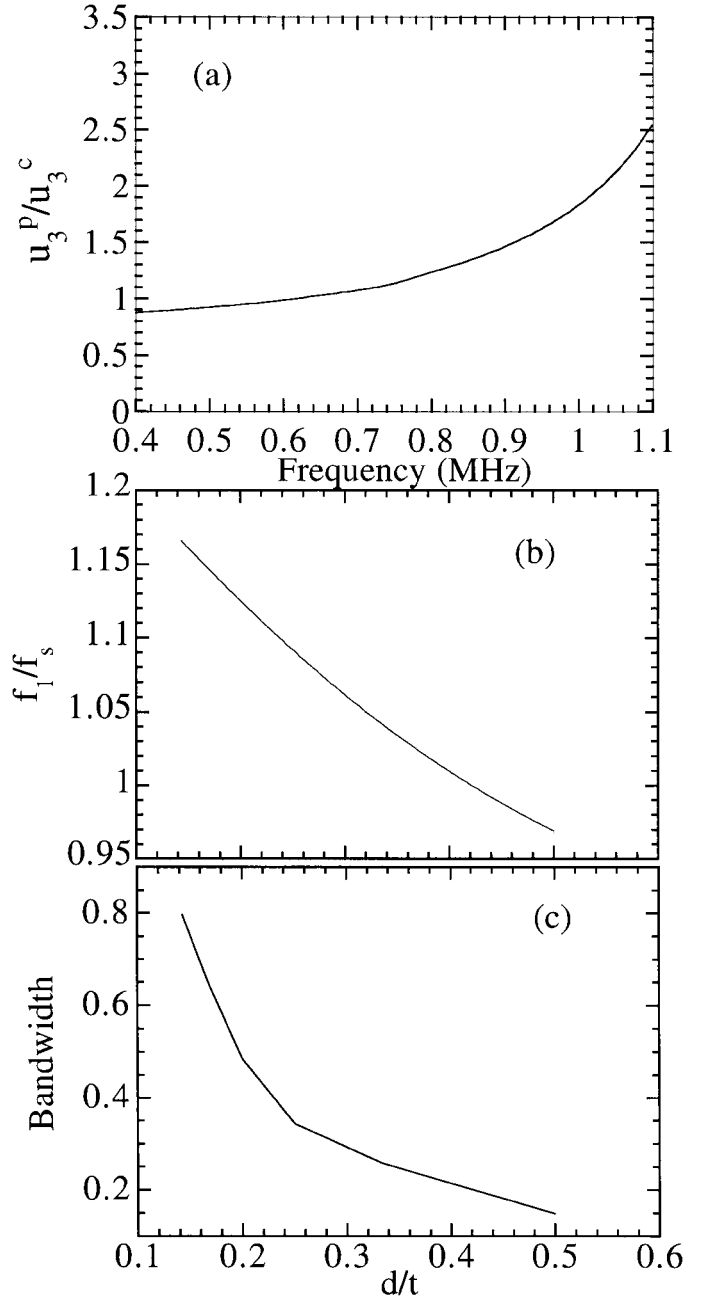


Fig. 12. (a) The ratio of  $u_3^P/u_3^C$  vs. frequency for a composite made of PZT-5H and Spurr epoxy (44% ceramic content) at a thickness of  $t/d = 4$  ( $d = 0.635$  mm) measured in water.  $u_3^P$  and  $u_3^C$  are the surface displacements at the centers of the polymer plate and ceramic plate, respectively. The results are derived from the model. (b) The ratio  $f_1/f_s$  as a function of  $d/t$  of the composite plate, where  $f_1$  is the frequency at which  $u_3^P/u_3^C = 1$  and  $f_s$  is the series resonant frequency for the thickness mode. The results are derived from the model. (c) The bandwidth as a function of  $d/t$  of the composite plate. The results here can be compared with those in Fig. 10 and apparently, the water loading improves the uniformity of the vibration profile at the composite surface. The results are derived from the model.

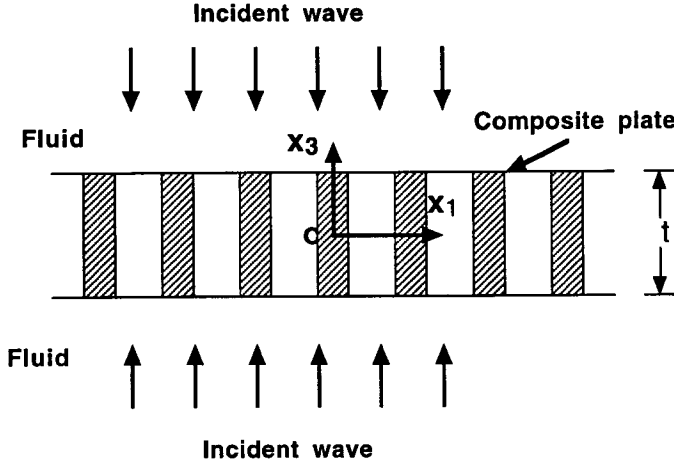


Fig. 13. Schematic drawing of a 2-2 composite plate under normal incident of a pressure wave from the water.

now the mode of  $\beta = 0$  should not be included since there is no externally applied electric field. To account for the incident wave in water, (27) is modified and the solutions in the  $x_3 > 0$  region are:

$$\begin{aligned}
 u_1^W &= j \sum_{n=0}^J h_n^W \sin(h_n^W x_1) \exp(j\beta_n^W x_3) R_n^W \\
 u_3^W &= -\beta_0 \exp(-j\beta_0 x_3) \\
 &\quad + \sum_{n=0}^J \beta_n^W \cos(h_n^W x_1) \exp(j\beta_n^W x_3) R_n^W \\
 T_3^W &= jT_0^W \left[ \exp(-j\beta_0 x_3) \right. \\
 &\quad \left. + \sum_{n=0}^J \cos(h_n^W x_1) \exp(j\beta_n^W x_3) R_n^W \right]
 \end{aligned} \quad (31)$$

where the term of  $-\beta_0 \exp(-j\beta_0 x_3)$  corresponds to the incident plane wave. By substituting (18), (19), and (31) into (30), we obtain a set of linear algebraic equations:

$$(M_{ij})(A_j) = (V_i) \quad (32)$$

where  $(M_{ij})$  is a  $15 \times 15$  matrix,  $(A_j) = (A_1, \dots, A_m, R_0^W, \dots, R^W)$  with  $m = 8$  and  $J = 6$ , and  $(V_i)$  is a  $15 \times 1$  matrix related to the incident wave. By solving (32) one can obtain all of the properties related to the behaviors of a composite plate under a harmonic acoustic pressure.

Shown in Fig. 14 is the open circuit voltage receiving sensitivity  $V/p$ , where  $V$  is the voltage output and  $p$  is the pressure of the incident wave, for a 44% 2-2 composite plate at the thickness resonance vs.  $d/t$  for the thickness resonance mode where the cross over region (point B in Fig. 2) is at  $d/t = 0.65$  [25]. That is, at  $d/t < 0.65$ , the thickness mode is in the first branch of the dispersion curves and above that, the thickness resonance is at the second branch of the dispersion curves where the polymer and ceramic vibrate out of phase. Since the problems treated in this paper are related only to the piezo-

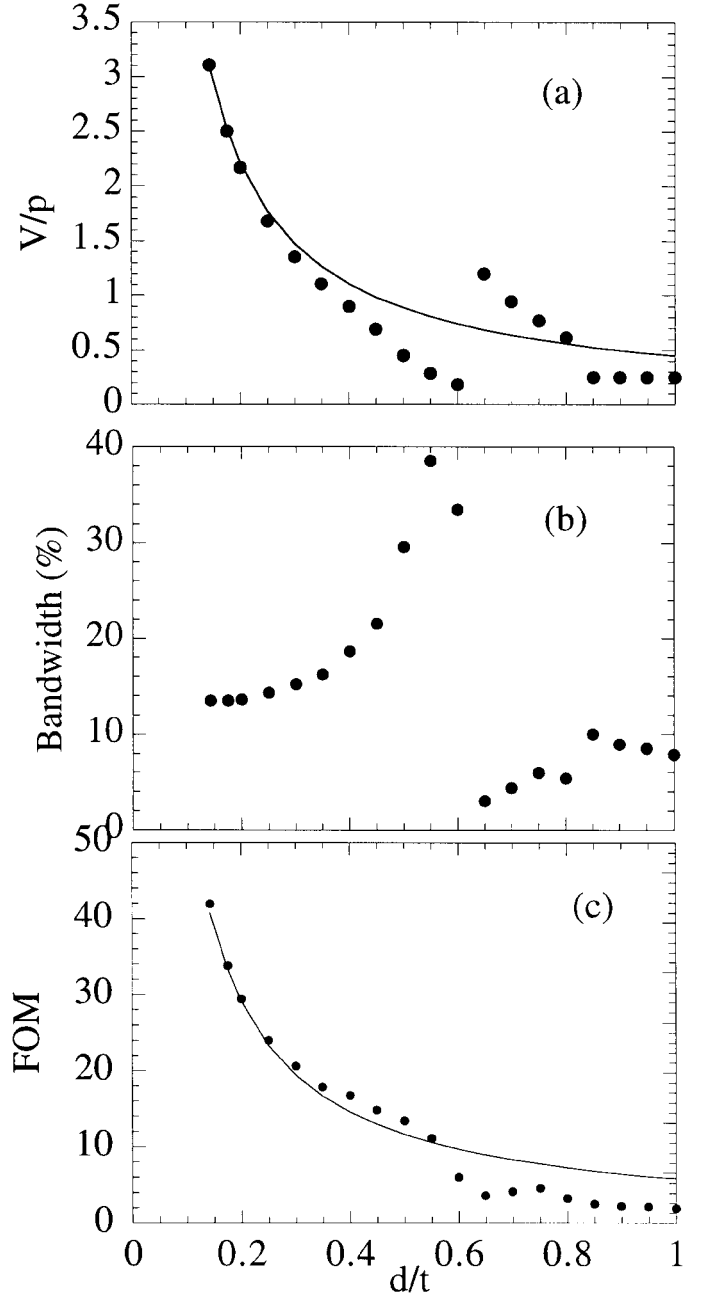


Fig. 14. (a) The influence of the unit cell dimension ratio of  $d/t$  on the open circuit voltage sensitivity of a 2-2 composite with 44% PZT-5H and Spurr epoxy matrix. Solid dots are  $V/p$  at the peak frequency ( $f_p$ ) and the solid line is the sensitivity of a single phase material with the effective properties of the composite. The results are derived from the model. (b) The 3 dB bandwidth as a function of  $d/t$  for a composite transducer derived from the model. (c) FOM (solid dots, the product of the sensitivity and the bandwidth) for the 2-2 composite in (a) as a function of  $d/t$ . The solid line is FOM for a single phase material with the effective properties of the composite. At  $d/t > 0.5$ , FOM drops much below the single phase material value. The results are derived from the model.

materials, the open-circuit receiving sensitivity is used here which, as pointed out by Kojima [25], is a system independent parameter. The bandwidth is defined as the 3 dB width about the peak frequency ( $f_p$  for the receiving mode). For a single phase material, it can be derived from the KLM model that the sensitivity here should be proportional to  $t$ , the thickness of the transducer. Hence, in Fig. 14, the  $V/p$  vs.  $d/t$  curve for a single phase material should fall off as  $t$  (solid line in Fig. 14) while the bandwidth should stay constant. The results show that the sensitivity of the thickness mode for a 2-2 composite decreases slowly as  $d/t$  becomes larger than 0.4, but the bandwidth increases gradually. The increase in the bandwidth is due to the merger of the two resonant modes in water. After that, there are anomalous changes in both the bandwidth and the sensitivity in the cross-over region. At higher values of  $d/t$  (thin composite plates), both the sensitivity and the bandwidth fall much below the values of single phase material (solid line). If we define the figure of merit (FOM) here as the product of sensitivity and bandwidth, as shown in Fig. 14(b), at  $d/t < 0.5$ , the FOM falls off with  $t$ . At  $d/t > 0.5$ , the FOM drops to much smaller value. Therefore, in order to gain a high receiving sensitivity and a broad bandwidth of a 2-2 composite transducer, it is desirable to have  $d/t$  less than 0.5. The results here can be compared with what is shown in Figs. 2, 8, 9, and 12. At  $d/t$  above 0.5, the coupling factor shows a precipitous drop (Fig. 9) and the thickness mode frequency also shows an apparent deviation from the extrapolated value (the dashed line in Fig. 2). Fig. 8 also shows that there is a significant coupling between the two modes. Although the results presented are for a composite with 44% ceramic content, it is approximately true for composites with other volume fractions.

## VI. SUMMARY

The details of a theoretical model on piezoceramic polymer composites with laminar periodic structure are presented. The result shows that the various resonant modes in a composite structure can be traced back to the modes in either an isolated ceramic plate or polymer plate with appropriate boundary conditions (stress free for the ceramic plate and strain free for the polymer plate). It also shows that there exist a series of modes associated with the periodic structure of a composite, which is beyond the stop-band edge resonance prediction. One of the main concerns in designing a composite transducer is how the surface vibration profile changes with frequency and how this is influenced by the aspect ratio  $t/d$ . It was predicted and verified by experiment that as long as the thickness resonance is below the first lateral mode frequency, there is always a frequency  $f_1$  which is near the thickness resonance and at which the polymer and ceramic vibrate in unison. The effect of  $t/d$  is to change the position of  $f_1$  with respect to the thickness resonance frequency and the bandwidth in which polymer and ceramic have nearly the

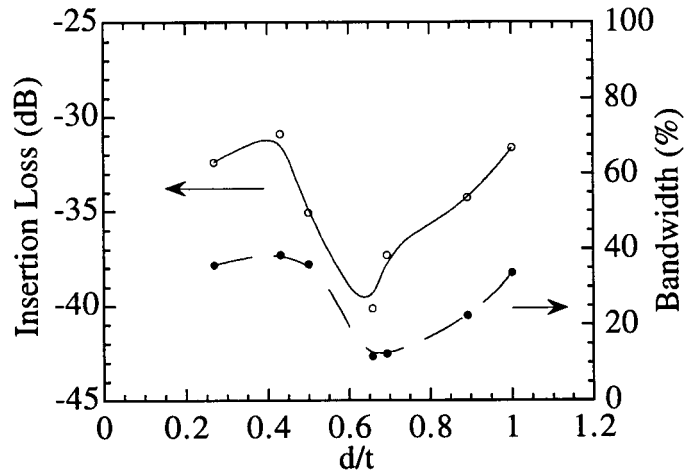


Fig. 15. The experimental data on the insertion loss (open circles) and 6 dB bandwidth (solid dots) of 2-2 composites with 44% volume content of PZT-5H and Spurr epoxy polymer matrix measured by the pulse echo method for different ratio of  $d/t$  ( $d = 0.635$  mm). The solid lines are drawn to guide eyes.

same vibration amplitude and phase. It is also predicted that, when operated in a fluid medium such as water, there will be a resonance mode whose frequency is determined by the velocity of the fluid medium and the unit cell length  $d$  and is associated with the oscillation of the fluid, causing the polymer and ceramic to vibrate  $180^\circ$  out of phase. The difference in the surface vibration profiles between in air and in water indicates the need to characterize the vibration pattern of a composite in a fluid medium since it is much closer to the real application environment.

In general, the maximum transmitting voltage sensitivity of a transducer is at a frequency near  $f_s$  and the maximum open circuit receiving sensitivity is near  $f_p$  of the thickness mode ( $f_p > f_s$ ), and hence it is expected that the influence of the lateral mode (hence, the aspect ratio  $t/d$ ) will be more severe on the receiving sensitivity. From the data analysis, it is shown that, when an FOM which is the product of the sensitivity and the bandwidth is introduced as the criterion of the performance of a composite transducer as a receiver, the performance deteriorates when  $d/t > 0.5$  for the composite discussed here. Experimental results confirm this finding where, as shown in Fig. 15, the insertion loss of a 2-2 piezocomposite shows large increases at  $d/t$  near and above 0.5.

## ACKNOWLEDGMENT

The authors wish to thank Dr. J. Yuan and Dr. H. Kunkel of ATL/Echo ultrasound for stimulating discussions.

## REFERENCES

- [1] W. A. Smith, "The application of 1-3 piezocomposites in acoustic transducers," *Proc. 1990 IEEE ISAF7*, Urbana, IL, 1990, pp. 145-152.

- [2] T. R. Gururaja, A. Safari, R. E. Newnham, and L. E. Cross, "Piezoelectric ceramic-polymer composites for transducer applications," in *Electronic Ceramics*, L. M. Levinson, Ed. New York: Marcel Dekker, 1987, pp. 92-128.
- [3] W. A. Smith and B. A. Auld, "Modeling 1-3 composite piezoelectrics: Thickness-mode oscillations," *IEEE Trans. Ultrason., Ferroelect., Freq. Contr.*, vol. 38, pp. 40-47, 1988.
- [4] K. Y. Hashimoto and M. Yamaguchi, "Elastic, piezoelectric and dielectric properties of composite materials," *Proc. IEEE Ultrason. Symp.*, Williamsburg, VA, 1986, pp. 697-702.
- [5] T. R. Gururaja, W. A. Schulze, L. E. Cross, R. E. Newnham, B. A. Auld, and J. Wang, "Piezoelectric composite materials for ultrasonic transducer applications. Part I: Resonant modes of vibration of PZT-rod-polymer composites," *IEEE Trans. Sonics Ultrason.*, vol. SU-32, pp. 481-498, 1985.
- [6] R. E. Newnham, D. P. Skinner, and L. E. Cross, "Connectivity and piezoelectric-pyroelectric composites," *Mater. Res. Bull.*, vol. 13, pp. 525-536, 1984.
- [7] B. A. Auld, H. Kunkel, Y. A. Shui, and Y. Wang, "Dynamic behavior of periodic piezoelectric composites," *Proc. IEEE Ultrason. Symp.*, Atlanta, GA, 1983, pp. 554-558.
- [8] B. A. Auld, Y. A. Shui, and Y. Wang, "Elastic wave propagation in three-dimensional periodic composite materials," *J. Physique*, vol. 45, pp. 159-163, 1984.
- [9] Y. Wang, E. Schmidt, and B. A. Auld, "Acoustic wave transmission through one-dimensional PZT-epoxy composites," *Proc. IEEE Ultrason. Symp.*, Williamsburg, VA, 1986, pp. 685-689.
- [10] Y. Wang, "Waves and vibrations in elastic superlattice composites," Ph.D. dissertation, Stanford University, CA, December 1986.
- [11] F. Craciun, L. Sorba, E. Molinari, and M. Pappalardo, "A coupled-mode theory for periodic piezoelectric composites," *IEEE Trans. Ultrason., Ferroelect., Freq. Contr.*, vol. 36, pp. 50-56, 1989.
- [12] M. Yamaguchi, K. Y. Hashimoto, and H. Makita, "Finite element method analysis of dispersion characteristics for the 1-3 type piezoelectric composites," *Proc. IEEE Ultrason. Symp.*, Denver, CO, 1987, pp. 657-661.
- [13] J. A. Hossack and G. Hayward, "Finite element analysis of 1-3 composite transducers," *IEEE Trans. Ultrason., Ferroelect., Freq. Contr.*, vol. 38, pp. 618-629, 1991.
- [14] A.-C., Hladky-Hennion and J.-N. Decarpigny, "Finite element modeling of active periodic structures: Application to 1-3 piezocomposites," *J. Acoust. Soc. Amer.*, vol. 94, pp. 621-635, 1993.
- [15] J. Sato, M. Kawabuchi, and J. Fukumoto, "Dependence of electromechanical coupling coefficient on the width to the thickness ratio of plate shaped piezoelectric transducers used in electrically scanned ultrasonic diagnostic systems," *J. Acoust. Soc. Amer.*, vol. 66, pp. 1609-1611, 1979.
- [16] Q. M. Zhang and X. Geng, "Dynamic modeling of piezoceramic polymer composite with 2-2 connectivity," *J. Appl. Phys.*, vol. 76, pp. 6014-6016, 1994.
- [17] Y. A. Shui, X. Geng, and Q. M. Zhang, "Theoretical modeling of resonant modes of composite ultrasonic transducers," *IEEE Trans. Ultrason., Ferroelect., Freq. Contr.*, vol. 42, pp. 766-773, 1995.
- [18] X. Geng and Q. M. Zhang, "Dynamic behavior of periodic piezoceramic-polymer composite plates," *Appl. Phys. Lett.*, vol. 67, pp. 3093-3095, 1995.
- [19] B. A. Auld, *Acoustic Fields and Waves in Solid*, New York: Wiley, 1973.
- [20] IEEE Standard on Piezoelectricity (ANSI/IEEE Standard 176-1987,1988).
- [21] H. F. Tiersten, *Linear Piezoelectric Plate Vibrations*, New York: Plenum, 1969.
- [22] C. G. Oakley, "Geometric effects on the stopband structures of 2-2 piezoelectric composite plates," *Proc. IEEE Ultrason. Symp.*, pp. 657-661, 1991.
- [23] Q. M. Zhang, S. J. Jang, and L. E. Cross, "High-frequency strain response in ferroelectrics and its measurement using a modified Mach-Zehnder interferometer," *J. Appl. Phys.*, vol. 65, pp. 2807-2815, 1989.
- [24] Q. M. Zhang, W. Cao, J. Zhao, and L. E. Cross, "Piezoelectric performance of piezoceramic-polymer composites with 2-2 connectivity: A combined theoretical and experimental study," *IEEE Trans. Ultrason., Ferroelect., Freq. Contr.*, vol. 41, pp. 556-562, 1994.
- [25] T. Kojima, "A new method for estimating the system-independent characteristics of an ultrasonic piezoelectric transducer," *Proc. IEEE Ultrason. Symp.*, pp. 649-654, 1981.



**Xuecang Geng** received the B.S. degree in physics from Xi'an Jiao tong university, Xi'an, China, in 1983 and the M.S. degree in acoustics from the Institute of Acoustics, Chinese Academy of Sciences, Beijing, China, in 1989. He is currently a candidate for the Ph.D. degree in Materials Research Lab, The Pennsylvania State University.

From 1983 to 1986 he was an engineer at Center of Microelectronics, Chinese Academy of Sciences, Beijing, China. This work focused on the computer aided design of integrated circuit and the computer modeling of integrated circuit and its processing. From 1990 to 1993 as a research assistant at Ultrasonic Lab of the Institute of Acoustics, he worked on the nondestructive evaluation of materials, acoustic wave logging, design, fabrication and characterization of 1-3 piezocomposite materials and ultrasonic transducers. From 1993 to 1995 as a research associate at Materials Research Lab of The Pennsylvania State University, he worked on the modeling of 2-2 and 1-3 piezocomposites. His current research interests are piezoelectric materials, ultrasonic transducers, and transducer array.

**Q. M. Zhang** was born in ZeiJian, China, in 1957. He received the B.S. degree in physics from Nanjing University, China, in 1981 and the Ph.D. degree in physics from the Pennsylvania State University, University Park, in 1986.

He is currently an Associate Professor of Electrical Engineering at the Materials Research Laboratory and Department of Electrical Engineering of the Pennsylvania State University. His research interests involve ferroelectric ceramic, polymer, and composite for actuator, sensor, and transducer applications; new design and modeling of piezocomposites; characterization of piezoelectricity and electrostriction and constitutive relations in ferroelectrics; smart materials and structures; novel, artificial, and nano-composite materials; effects of defect structure on the dielectric, piezoelectric, and elastic properties of ferroelectric materials. From 1986 to 1988, he was a Post-Dr at Materials Research Laboratory of Penn State. From 1988 to 1991, he was a research scientist at Brookhaven National Laboratory, NY, conducting research on interface, surface, and thin films with neutron and synchrotron X-ray scattering techniques.

Dr. Zhang is a member of the American Ceramic Society, IEEE, American Physical Society, and Materials Research Society.